A probabilistic framework for fatigue damage of lift based wave energy converters

Abel Arredondo-Galeana, Paul Lamont-Kane, Weichao Shi, Matt Folley and Feargal Brennan

***Abstract*—Lift based wave energy converters (WECs) have shown great potential to harness the energy of the waves. This type of device extracts energy using wave-driven rotating foils in regular or irregular waves. However, as with all wave energy converters, lift based WECs are exposed to variable loading which may result in premature mechanical failure. Therefore, it is important to develop efficient fatigue analysis tools that help in predicting the lifetime of lift based WECs. In this paper, we test the hypothesis that when lift based WECs operate at constant rotational velocity in irregular waves, fatigue damage can be computed through a probabilistic approach. We consider a sample stress hot spot in the hydrofoils of the WEC. We compare the fatigue damage computed using a probabilistic approach with the damage computed using well established deterministic methods. We find that for sea states of high likelihood of occurrence, the probabilistic method is a useful tool in determining fatigue damage. This is a promising outlook since it confirms that the fatigue damage of lift based wave devices can be treated in a similar fashion to the fatigue damage of traditional offshore structures.**

***Index Terms*—Lift based WEC, fatigue damage, wave cycloidal rotor, wave energy**

I. Introduction

OFFSHORE structures are at risk of mechanical failure due to variable loading on the structures caused by the harsh marine environment. Hence, great effort has been invested towards the development of methods that quantify and help preventing fatigue damage of offshore structures [1].

Wave energy converters (WECs) are no different to offshore structures in that they are also subject to random loading due to the variability of ocean waves. However, the loading mechanisms on WECs can be more complex due to moving parts and the unique structural hydrodynamic relationships of each wave energy converter.

© 2023 European Wave and Tidal Energy Conference. This paper has been subjected to single-blind peer review.

This work was supported in part by the European Union Horizon 2020 Innovation and Research Programme under grant 851885.

A.A.G and F.B are with the Department of Naval Architecture, Ocean and Marine Engineering at the University of Strathclyde, Glasgow, UK, (e-mail: abel.arredondo-galeana@strath.ac.uk, feargal.brennan@strath.ac.uk).

P. L. K. is with the School of Natural and Built Environment, Environmental Change and Resilience, Queen's University Belfast, Belfast, UK (e-mail: p.lamont-kane@qub.ac.uk).

W. S. was with the Department of Naval Architecture, Ocean and Marine Engineering at the University of Strathclyde, Glasgow, UK. He is now in Newcastle University (e-mail: weichao.shi@newcastle.ac.uk).

M.F. is with Applied Renewables Research, Belfast, UK (e-mail: m.folley@arrltd.co.uk).

Digital Object Identifier:
https://doi.org/10.36688/ewtec-2023-393

Despite the loading complexity of WECs, developing models to quantify fatigue damage in these devices remains a concern to any wave energy developer. Accurate fatigue damage models can help, for example, to develop a resilient and cost effective structural WEC and therefore, to reduce its levelised cost of energy. Consequently, it is necessary to develop analytical models that are helpful during the design stage of a WEC to assess and quantify fatigue damage of WEC structures.

In this paper, we focus on lift based WECs. In this type of WECs, lift forces are generated through rotating hydrofoils. The foils, and specifically the lift forces, drive the rotation of a central shaft and this kinetic energy is converted to electrical energy. Although, lift based WECs have the capacity to operate fully submerged and use passive or active pitch control to mitigate load oscillations in the hydrofoils, the variation in loading cannot be completely eliminated due to the randomness and variability of individual waves within sea states. Therefore, the structures of lift based WECs, in particular the hydrofoils, are subject to fatigue.

We formulate the hypothesis that provided that a lift based WEC is operated at constant rotational speed in a given sea state, then fatigue damage on its hydrofoils can be computed through a probabilistic approach. We test our hypothesis by comparing the fatigue damage results of the proposed probabilistic approach to results computed with deterministic methods, namely: Miner's rule and the equivalent stress method. To estimate the loads on the hydrofoils, we consider irregular sea states and implement a potential flow single point vortex model [2]–[5].

Probabilistic fatigue approaches have been developed successfully for offshore structures [1], [6], because although sea states are of variable nature, they are statistically invariant, i.e. they can be characterised through a signature wave energy spectrum. Probabilistic approaches offer the advantage of containing the fatigue stress information in energy spectra, which can be easily correlated to the energy spectra of a particular sea state. These correlations promote the formulation of wave-to-damage design relationships. However and surprisingly, to this date and to the knowledge of the authors of this paper, the application of probabilistic methods to wave energy converters remains vastly unexplored. In particular, for lift based WECs that operate at constant velocity in irregular waves, we speculate that a fatigue probabilistic approach can render useful results. Note that a probabilistic fatigue damage method has never been tested or developed for lift based WECs. Hence, this is the focus of this

study.

The structure of the paper is as follows. First, we introduce the concept of a lift based WEC, specifically a wave cycloidal rotor. Then, we identify the sample stress hot spot in the hydrofoils of the rotor. Subsequently, we present the theoretical framework for the probabilistic and the deterministic fatigue analysis methods. We then assess both probabilistic and deterministic methods for a different range of conditions, and present the conclusions of this work.

II. Lift based wave energy converters

A tethered bottom based lift based WEC is depicted in Figure 1. The rotor is anchored to the sea bed with tethered tensioned legs that are assumed to fully restrain motion in surge, sway, heave, pitch, roll and yaw. The rotor consists of two hydrofoils and a central shaft, which are connected to circular end plates. Note that the design of the rotor shown in Figure 1 is similar to the design of the lift based WEC of the Atargis corporation, with the difference that their design uses telescopic v-frames to anchor the device to the seabed [2], [7]. Although variations in design of lift based WECs exist [8], the rotor and stator are common in these devices.

The stator, which is the structural part that does not move, is composed of two cylindrical nacelles. The nacelles house the generator and the pitching mechanisms of the hydrofoils. The rotational velocity of the hydrofoils in combination with the wave particle velocity generates an inflow and an angle of attack, and therefore lift and drag forces are generated in each hydrofoil. Provided that the lift to drag ratio of the hydrofoils remains high, the rotation of the hydrofoils drive the central shaft, and mechanical power is converted to electrical power.

The rotational phase, or rotational speed, are controlled in regular [5], [9] or irregular sea states [10], respectively, to produce positive power. In regular sea states, the rotational frequency of the rotor is the same as the frequency of the incoming wave. However, a phase angle between rotor and wave is necessary to generate lift in the foils. In contrast, in an irregular sea state, because the phase of rotation of the rotor is difficult to compare to the phase of a random sea state, then the rotational speed is defined as a fraction of the peak frequency of a JONSWAP spectrum [10]. Note that for every irregular sea state, there is a fixed rotational speed that can maximise power output under fixed speed conditions [10], [11].

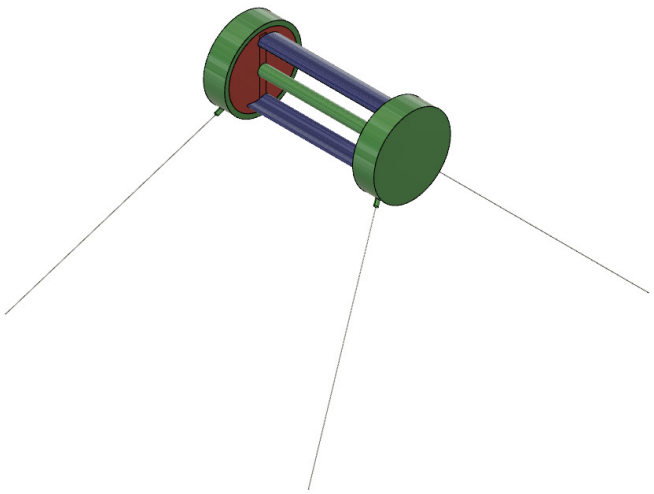

Fig. 1. LiftWEC wave bladed cyclorotor in operation near water surface and supported by two v-frames

III. Hydrodynamic and structural modelling

The hydrodynamic forces on the hydrofoil of the cyclorotor are modelled by representing the foil as a point vortex under a free surface. This representation has been used in the literature of lift based WECs to model free surface elevation [3], [7], [12] and recently, to model loads on the hydrofoils of the cyclorotor [4], [5], [13].

The single point vortex is a potential flow representation of the hydrofoil to estimate its inflow velocity and angle of attack. Specifically, the inflow velocity U is considered to be the vectorial sum of the wave velocity w, the velocity component due to a point vortex under a free surface q and the velocity due to the rotation of the hydrofoil v. Figure 2 shows the schematic representation of w, q, v and U. The angle of attack α is measured as the angle between v and U. Once α and U are known, the lift and drag coefficients of the hydrofoil are determined through a look up table. Subsequently, the lift and drag forces on the hydrofoil can be determined. In this work, look up tables of a symmetric NACA 0015 foil are used [14]. The tables are interpolated to account for different Reynolds numbers.

We describe now, the procedure to compute w, q, v, U and α, which are the vectors and the angle shown in Figure 2. The wave velocity component w is computed assuming irregular waves, by discretising a JONSWAP wave spectrum in frequency. Individual waves of amplitude A_j are considered, where j is the index of each discrete wave. The wave spectrum is discretised to compute A_j, following [15], [16], such that

$$A_j = \sqrt{2 S_A(\omega_j) \Delta\omega}, \tag{1}$$

where $S_A(\omega_j)$ is the amplitude of the spectrum at ω_j, and $\Delta\omega$ is the discretisation step of the spectrum. Then, the velocity components of each j-th wave is computed assuming linear deep water wave theory [17], such that

$$w_{x,j} = \frac{\pi A_j}{T} e^{k_j y} \cos(k_j x - \omega_j t + \eta_j) \tag{2}$$

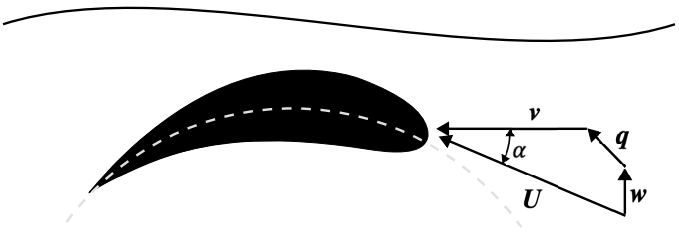

Fig. 2. Velocity vector diagram on foil of cyclorotor.

and

$$w_{y,j} = \frac{\pi A_j}{T} e^{k_j y} \sin(k_j x - \omega_j t + \eta_j), \tag{3}$$

where A_j, k_j, ω_j and η_j are the wave height, number, angular frequency, and phase of the j-th frequency component, respectively, and x, and y are the horizontal and vertical positions of the hydrofoil.

Each k_j is computed with $k_j = 2\pi/\lambda_j$, where λ_j is the wavelength of each discrete frequency component [18]. The phase of each component η_j is randomly assigned within a range of 0 to 2π radians. The total wave velocity component w_x and w_y is the sum of all the j-th wave velocity components, which are denoted in Equations (2) and (3).

The position of the foil around the central shaft is defined in terms of the angular position of the foil, such that

$$x = r\cos(\theta(t) + \psi) \tag{4}$$

and

$$z = -r\sin(\theta(t) + \psi) + z_0, \tag{5}$$

where z_0 is the submergence of the rotor and defined negative from the mean sea level (MSL) to the center of the central shaft, $\theta(t)$ is the angular position measured with respect to the positive horizontal axis and positive clockwise ([3], [10]) and ψ denotes the starting position of the foil with respect to the positive horizontal axis. For the case of a two foil rotor, as the one considered in this work, $\psi = 0$ and $\psi = \pi$, for the first and second hydrofoil, respectively. Hence, the velocity component due to the rotation of the foil around the central shaft of the rotor is given by

$$u_x = -\omega r\sin(\theta(t)) \tag{6}$$

and

$$u_z = -\omega r\cos(\theta(t)), \tag{7}$$

where ω is the rotational frequency of the rotor. Note that the induced velocity due to the rotation of the point vortex is $-\mathbf{u}$, therefore we consider $-u_x$ and $-u_z$.

The complex potential of a single vortex under a free surface was derived by [19]. By utilising the Dawson's function [3], the complex potential becomes

$$F(x,t) = \frac{\Gamma(t)}{2\pi i}\mathrm{Log}\left[\frac{x-\zeta(t)}{x-\zeta'(t)}\right] + -\frac{2i\sqrt{g}}{\pi}\int_0^t \frac{\Gamma(\tau)}{\sqrt{i(x-\zeta'(\tau))}} D\left[\frac{\sqrt{g}(t-\tau)}{2\sqrt{i(x-\zeta'(\tau))}}\right] d\tau, \tag{8}$$

where the first term represents the single point vortex and its mirror vortex above the free surface, and the second term represents the memory term on the free surface due to the presence of the vortex throughout the rotation interval $t-\tau$, where t is the current time step and τ is the memory time constant. In this work, $\tau = T$, following [5].

The complex velocity of Equation 8 is

$$\frac{\partial F(x,t)}{\partial x} = \mathbf{q} = q_1 - iq_1 + q_2 - iq_2, \tag{9}$$

where 1 and 2, refer to the first and second term of Equation 8, respectively. The explicit terms for Eq. 8 for a two foil lift based WEC are available in [3].

With w, u and v determined, the angle of attack α is defined as the angle between the inflow velocity $\mathbf{U}$ and the rotational velocity of the rotor $\mathbf{v}$, such that

$$\alpha = \sin^{-1}\left[\frac{||\mathbf{U}\times -\mathbf{v}||}{||\mathbf{U}||||-\mathbf{v}||}\right], \tag{10}$$

in agreement with α shown in Figure 2. The lift and drag forces of the hydrofoil are defined as

$$L = \frac{1}{2}C_L\rho csU^2 \tag{11}$$

and

$$D = \frac{1}{2}C_D\rho csU^2, \tag{12}$$

respectively, where C_L is the lift coefficient, C_D is the drag coefficient, ρ is the fluid density, c is the chord length of the foil, s is the span and U is the magnitude of the inflow velocity on the foil. The tangential force on the hydrofoil is

$$T = L\sin\alpha - D\cos\alpha \tag{13}$$

and the radial force is

$$R = L\cos\alpha + D\sin\alpha. \tag{14}$$

In this work, we utilise Equation (14), as the input to compute the bending stresses σ of the hydrofoil hot spot. We approximate the spar section of the hydrofoil as a square hollow section, as illustrated in Figure 3a. The spar is the section of the hydrofoil where the path of the radial force is exerted, i.e. the radial force acts at the quarter chord position of the foil [5].

The bending moments M along the spar of the hydrofoil can be estimated through beam theory, by considering a fixed beam. Assuming a uniform distributed load W, then

$$W = R/l, \tag{15}$$

where l is the span of the foil.

The static equilibrium equations of the beam are solved and the bending moments M are computed. As an illustrative example and assuming uniform radial loading, we tested 16 different hydrofoil span values, from 0 to 15 m, in steps of 1 m, at a fixed rotor radius (R=10 m). The distributions of the normalised moments (M[-]) versus normalised span lengths (s [−]) are shown in Figure 3b. In Figure 3b, the blue, red and dotted lines represent the longest, shortest and intermediate tested spans, respectively. Results are solved analytically in software Python. Figure 3b shows that the maximum M occurs at the fixed ends of the beam and therefore, these are the locations of the hot spot stresses.

Lastly, the bending stresses σ are computed at one of the fixed ends of the hydrofoil, such that

$$\sigma = \frac{My}{I_{xx}}, \tag{16}$$

where M is the bending moment at the stress hot spot, y is the distance from the centroid to the outermost section of the cross section, and I_{xx} is the second moment of area of the cross section.

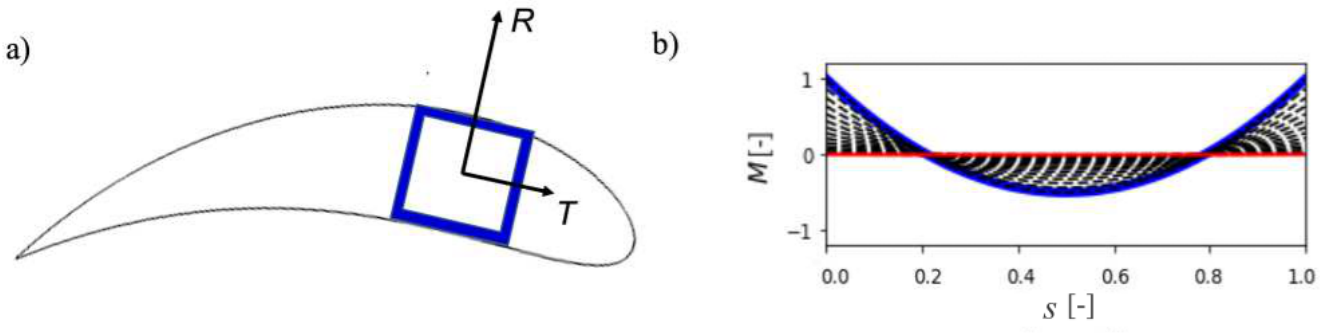

Fig. 3. a) Hydrofoil spar section represented with square hollow section (SHS) in blue and b) normalised bending moment (M [−]) distributions versus normalised span lengths (s [−]), where, M [−] is plotted for span lengths over a range of 0 (red line) to 15 m (blue line), with intermediate steps of 1 m (dotted lines). Computations consider a square hollow section.

IV. Probabilistic Fatigue Methods

Probabilistic fatigue methods are widely used in offshore engineering. For time varying processes, probabilistic methods are able to capture the energy footprint of the stresses, which is essential to obtain accurate estimates of fatigue damage [1], [20]. Furthermore, probabilistic methods allow time varying processes to be analysed as stationary processes, which allows the application of statistical analysis of energy spectra. Hence, in this work, we postulate the hypothesis that the fatigue damage of a lift based WEC operating at constant speed in irregular waves is statistically stationary, and therefore, fatigue damage can be estimated with a probabilistic approach.

In a probabilistic framework, the yearly damage D_i on a stress hot spot in a given i-th sea state is given by

$$D_i = \frac{n_i}{N_i} = \int_0^\infty \frac{365 \times 24 \times 3600 P_i f_0 f_i(\sigma) dS}{K/S^m}, \quad (17)$$

where P_i is the probability of occurrence of the i-th sea state, $f_i(\sigma)$ is the probability density function of σ and f_{0i} is the zeroth mean frequency or crossing up frequency, which is defined as

$$f_{0i} = (1/2\pi)\sqrt{m_{2i}/m_{0i}}, \quad (18)$$

where m_{0i} and m_{2i} are the zeroth and second order stress spectral moments, respectively. In Equation (17), K, S and m are values derived from the SN curve of a specific material. In this case, we consider hydrofoils fabricated with offshore steel with cathodic protection. Note that for the sea states considered in this work, in Equation (17),

$$\int_0^\infty f_i(\sigma) dS = 1. \quad (19)$$

To solve Equation 18, the n-th spectral moment of the i-th sea state is defined as

$$m_{ni} = \int_0^\infty \omega^n G_{yyi}(\omega) d\omega, \quad (20)$$

where $G_{yyi}(\omega)$ is the hot spot stress energy spectrum and ω is the wave frequency. In Equation (20), it can be seeen that the zeroth spectral moment m_{0i} is the the area under $G_{yyi}(\omega)$.

In this work, $G_{yyi}(\omega)$ is defined as the squared of the Fourier transformation of the hot spot stress time series, such that

$$G_{yyi}(\omega) = [\sigma(f)]^2, \quad (21)$$

where $\sigma(f)$ is the Fourier transform of $\sigma(t)$.

The spectral width parameter κ is used to determine the width of G_{yyi}, such that

$$\kappa = \sqrt{1 - \frac{m_2^2}{m_0 m_4}}, \quad (22)$$

where $\kappa = 0$ indicates a narrow band spectrum. This is a useful metric to characterise and understand the stress spectra of lift based wave energy converters.

The lift based WEC of this study is conceptually designed to operate in the Atlantic coast of France. Figure 4 shows the scatter plot data corresponding to a point in the North Atlantic at the coast of France, located at 47.84° N, 4.83° W. The figure shows T_e along the horizontal axis and H_s along the vertical axis. The data is available from the Ifremer FTP server and contains directional spectral wave data for 10-years between 2000-2010 [21]. The conversion from T_p to T_e is performed through $T_e = \alpha T_p$, where $\alpha = 0.9$ for a JONSWAP wave spectrum [22]. Hence, considering the data from Figure 4, we consider a design sea state with $T_p = 8\,\text{s}$ and a wave height of $H_s = 2$ m.

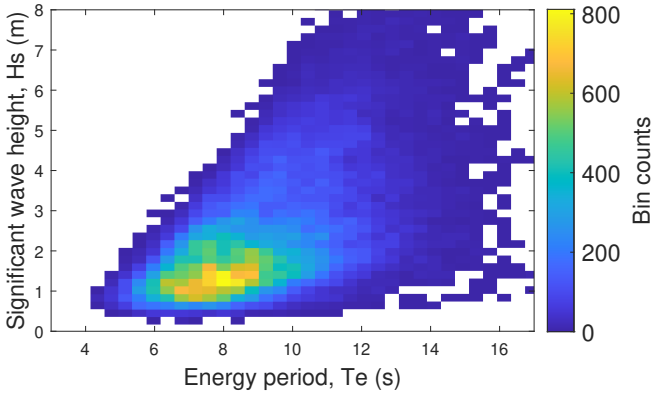

Fig. 4. Scatter plot showing energy period T_e versus significant wave height H_s of seasonal data of one point in the Atlantic coast of France

V. Deterministic fatigue methods

Fatigue damage can be quantified in a deterministic manner, through Miner's rule. The rule postulates that the total damage is a linear summation of fraction damages. The total damage is defined as

$$D = \sum_{i=1}^{n} \frac{n_i}{N_i}, \tag{23}$$

where D is the total damage to the structure, n_i is the number of cycles at $\Delta\sigma_i$, where $\Delta\sigma$ is a stress range and i is the index of $\Delta\sigma$, N_i is the number of cycles to failure at $\Delta\sigma_i$ and n is the total number of $\Delta\sigma$ present in a stress time series. The number of cycles to failure for a particular $\Delta\sigma$ can be obtained from the SN curve of the specific material. In this work, we assume the C curve for offshore steel in seawater with cathodic protection. The curve is shown in Figure 5.

The SN curve represents the relationship between number of cycles to failure at a particular $\Delta\sigma$. The relationship is given by

$$\log \mathrm{N} = \log \overline{a} - m \log \Delta\sigma, \tag{24}$$

where $\overline{a}$ is the intercept of the curve on the horizontal axis and m is the negative inverse slope of the curve. Figure 5 shows that the curve has two slopes and that the inflection point of the slopes occurs approximately at a $\Delta\sigma$ of 83 MPa.

For variable loading and long time series, it is useful to derive an equivalent stress range $\Delta\sigma_{eq}$ to compute the damage in the structure and increase computational efficiency. $\Delta\sigma_{eq}$ can be expressed such that

$$\Delta\sigma_{eq} = \left[\sum_{i=1}^{m} \gamma_i (\Delta\sigma)^{-1}\right]^{-1/m}, \tag{25}$$

where γ_i is the portion of the stress range $\Delta\sigma_i$ in the total cycle time history. Then, we can compute an equivalent number of cycles N_{eq} to failure, assuming $\Delta\sigma_{eq}$ and using Equation (24).

The last step of the equivalent stress range approach is to determine D. By considering the total number of cycles n_t of the stress time series and N_{eq}, we can define

$$D = \frac{n_t}{N_{eq}}. \tag{26}$$

VI. Results

A. Regular waves

As a first exploratory case to compare deterministic and probabilistic fatigue methods, we simulate the wave cycloidal rotor in a regular sea state. We note however, that the probabilistic fatigue damage quantification is not expected to be meaningful in regular sea states, since the purpose of the probabilistic approach is to rely on a time variable stress signal, which has a statistically invariant response. However, studying the regular sea state case can shed light into the loading properties of the rotor. Furthermore, it can serve as a useful initial evaluation of the capabilities of the probabilistic method versus deterministic fatigue approaches. Therefore, we show this case first. The hydrodynamic forces on the foils of the rotor are computed and the fatigue damage due to R in one of the hydrofoils is analysed. The radius of the rotor is 6 m, the hydrofoil chord length is 6 m, the span is 10 m and the submergence is -10 m. The incoming wave is defined with a period of $T = 8\,\mathrm{s}$ and a wave height of $H = 2$ m.

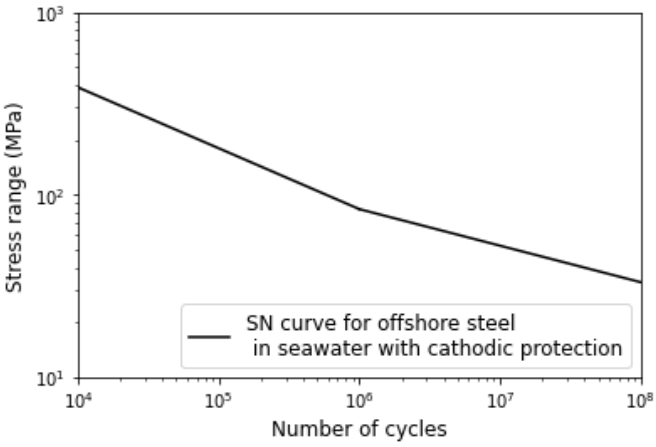

Fig. 5. SN curve for offshore steel in seawater with cathodic protection.

A time series of 10 minutes, i.e. 600 seconds, is simulated. The time series of the radial force R of one of the hydrofoils is converted into a time series of stress ranges $\Delta\sigma$, following the procedure described in Sec. III and in Arredondo et al. [5]. The computed stresses σ are shown in Figure 6a. It can be seen that the σ ranges approximately between 20 MPa to 42 MPa, i.e. $\Delta\sigma \approx 22$ MPa. The oscillations are periodic. The Fourier transform of σ is shown in Figure 6b. Figure 6b highlights three frequency peaks. The first peak is located at 0.79 Hz and is associated to the rotational frequency of the rotor and the wave frequency.

The second peak is a harmonic occurring at twice the frequency of the first peak. The harmonic indicates a consistent and constant modification of the fundamental waveform. Hence, the σ signal, although periodic, is not completely sinusoidal. In fact, the angle of attack oscillation of the cyclorotor is skewed and can be approximated with three sinusoidal curves, as demonstrated in the Fourier series decomposition shown in [5]. The asymmetry of the signal in regular waves is namely due to the change in depth of the foil throughout one period of rotation. Lastly, the third peak is associated to the radiated wave component. This third peak, which occurs at three times the fundamental wave frequency vanishes when the term q, from Equation 8, is not included in the radial force computation.

The computed damage D with the Miner's rule and the equivalent stress method yield the same results. Note, however, that for the equivalent stress method, the grouping factor γ_i from Equation (25), needs to be carefully selected and tuned to yield the same results as Miner's rule. Hence, γ_i is determined by iteration and

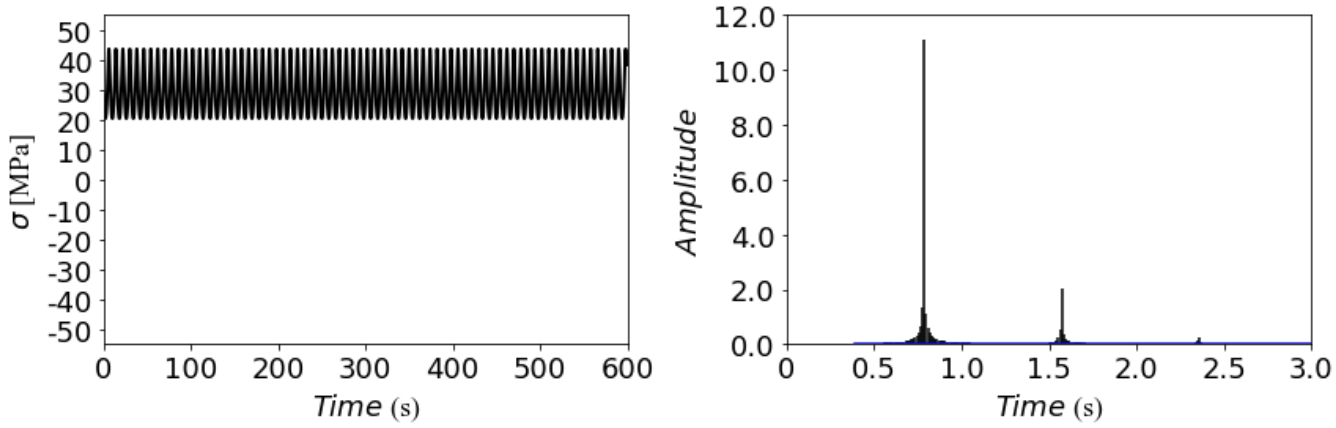

Fig. 6. Regular sea state case showing a) bending stresses time series in foil stress hot spot and b) energy spectrum of stress signal

by finding the convergence value, where the method reaches an asymptotic D value, which is the same value computed with Miner's rule.

In contrast, D computed with the probabilistic method underestimates D by about 20% with respect to D computed with the deterministic methods. It is found that, in regular waves, the discrepancy of probabilistic and deterministic methods is mostly due to the presence of the second term of Equation (8). This term causes the third harmonic in the Figure 6b, and causes the probabilistic method to lose accuracy. Note that the second term of Equation (8), accounts for for the memory term of the effect of the foil circulation in the free surface [5], and when this term is considered, the spectra width parameter is $\kappa \geq 0.5$. Conversely, when the second term of Equation (8) is not considered, i.e., when the width of the spectra is reduced and $\kappa < 0.5$, the comparison of probabilistic and deterministic D lies within 4%.

Although the hydrodynamic model accuracy does not depend of the second term of Equation (8), but rather on the limitations of a potential flow model to predict unsteady and separated flows [5], it is understandable that the damage computation in a regular sea state with a probabilistic method is not of practical use, as it would be in an irregular sea state scenario. Hence, we expect that discrepancies between probabilistic and fatigue methods decrease in irregular sea states scenarios, where the input to the hydrodynamic model is a JONSWAP wave spectrum. We present the results for irregular waves in the following sections.

B. Irregular waves

Narrow band energy spectra: We compare the damage computation methodologies in a narrow band sea state. We produce a narrow-band spectrum by considering the definition of a JONSWAP wave energy spectrum, but constraining the number of waves and the range of frequencies. The range of frequencies are defined around the peak frequency ω_p of the wave spectrum. Hence, we utilise 10 discrete waves with a range of frequencies distributed over the interval $0.9 \leq \omega_p \leq 1.1$. For this study, $\omega_p = 2\pi/T_p$, and therefore the rotor operates at the peak frequency of the wave spectrum. In this case, we consider $T_p = 8$ s and $H_s = 2$ m, as defined in Sec. IV.

For the irregular sea state scenario, the simulations are run for 1 hour, i.e. 3600 seconds. The time series of the computed σ is shown in Figure 7a, whilst the stress spectrum $G_{yyi}(\omega)$ is shown in Figure 7b. Note that the spectrum is plotted between $0.5\omega_p$ and $10\omega_p$. Increasing this range further did not alter the computed D with the probabilistic method. Therefore, this was the minimum acceptable ω range at which the probabilistic method showed convergence.

Figure 7a shows the computed time series of σ. Noteworthy, Figure 7a shows that σ oscillates around a mean value of 0 MPa. The zero stress mean value contrasts the non zero mean value of the regular sea state. However, in an irregular sea state, a zero stress mean value is to be expected, since at constant speed in irregular waves, the inflow angle on the foil continuously changes direction. In fact, as shown in [10], the mean α in an irregular sea state is $\alpha = 0°$, and therefore, there are important implications in designing systems that operate around a zero angle or zero stress mean value [10]

Figure 7b shows the stress spectrum $G_{yyi}(\omega)$ computed from the time series of σ shown in Figure 7a. In Figure 7b, the highest ω_p peak corresponds to the carrier frequency, which is equal to the peak frequency of the wave spectrum. Note that even though we used 10 discrete frequencies in the range $0.9 \leq \omega_p \leq 1.1$ to generate the wave spectrum, further peaks appear to the right of the ω_p peak. These additional peaks are associated to harmonics of the signal. As those identified in the regular sea state test.

To obtain a statistically meaningful result between probabilistic and fatigue methods, we performed 20 simulations of 3600 seconds. We then averaged the differences between methods. The computed D with the probabilistic method was on average, within 12% from the D computed with the deterministic methods. Although the wave spectrum was defined as narrow band, the average bandwidth of the stress spectra was $\kappa = 0.73$. This is due to the additional harmonics shown in Figure 7b. Nonetheless, although the stress

spectrum is not narrow band, for the case when the input wave spectrum is narrow band, the probabilistic method shows satisfactory results.

Broad band energy spectra: We now test the case of an input broad band wave energy spectrum interacting with the rotor. We consider, initially, a total of 10 discrete waves to generate the wave spectrum. Specifically, the band of the spectrum extends over the interval $0.5 \leq \omega_p \leq 2.5$, where ω_p is the peak wave frequency.

Figure 8a shows the computed time series of σ in the hydrofoil hot spot. Similarly to the narrow band irregular wave case, the stress signal oscillates around a mean value of 0 MPa. This is because the angle of attack of the foil oscillates a mean zero angle of attack. Figure 8b shows the stress energy spectrum. The shape of the spectrum is more of a Gaussian type. Note that the dominant frequency is shown by the highest peak at ω_p =0.79 Hz.

We performed 20 simulations of 1 hour duration to generate a statistically significant D computation. We compare the probabilistic results to that computed with the deterministic methods, namely Miner's rule and the equivalent stress approach. For this broad band wave energy spectrum case, the agreement between the probabilistic and deterministic D value lies within 2%. This is a significant improvement over the narrow band case, and shows that for a more realistic input of wave conditions, the probabilistic approach is a robust tool for D computation.

Lastly, we compute D for the case of a broad band JONSWAP energy spectrum formed by 80 discrete waves. The band of the JONSWAP spectrum extends over the inreval $0.5 \leq \omega_p \leq 2.5$, where ω_p is the peak wave frequency. Figure 9a shows the time series of bending stresses around the foil hot spot. The mean value of stresses in this case is also 0 MPa. In contrast to the narrow band and the 10-discrete wave broad band spectrum, Figure 9b shows a Gaussian shape. In fact, the shape of the spectrum of Figure 9b, resembles also the shape of the JONSWAP wave spectrum. Fatigue damage D is computed with the deterministic methods and the probabilistic method. A total of 20 simulations of 1 hour duration are run and the ratio between deterministic and probabilistic methods is computed and averaged. For this broad band energy spectrum case, the agreement between D computed between the probabilistic and deterministic methods lies within 2%.

These results highlight the validity of the hypothesis postulated at the beginning of this study. A probabilistic approach to compute D can be applied to lift based WECs that operate at constant velocity in broadband irregular sea states. We recall that in this case, D is computed at one of the hydrofoil's stress hot spots. However, it is envisioned that the methodology is applicable to other stress hot spots of the cyclorotor, and therefore, has a great potential for future fatigue related studies.

In the next Section, we summarise the results obtained for the different type of wave energy spectra. We used the multiple discrete wave broad band spectrum, i.e. the best and more realistic scenario, to compare the ratios between probabilistic and deterministic approaches for a range of different sea states. This with the aim to understand whether the probabilistic approach is robust when tested in different sea state conditions.

Summary of shape of spectrum effects: We summarise the results presented in Section VI-B, with fuzzy terminology [23] to highlight the applicability of the probabilistic method to compute D at the hydrofoil stress hot spot. We recall that the wave cycloidal rotor is assumed to operate at constant rotational speed ω, where $\omega = 2\pi/T_p$. Note, however, that this value can be adjusted and optimised for power production [10], [11], provided that it remains constant through every sea state. For this preliminary assessment, the selected sea state, at which the rotor operates, is one with a high probability of occurrence, i.e. $H_s = 2$ m and $T_p = 8$ s, where $P_i \approx 0.15$. This is highlighted in Figure 4.

In Figure 10, we assess and present damage ratio between the probabilistic approach and deterministic approach (Miner's rule), and classify the agreement as very good ($D_{prob}/D_{det} \geq 0.95$), good ($D_{prob}/D_{det} \geq 0.85$), medium ($D_{prob}/D_{det} \geq 0.75$) and bad ($D_{prob}/D_{det} < 0.75$). Figure 10 shows that the probabilistic method works better with broad band wave energy spectra, either with a wide or narrow number of discrete waves.

In the next Section, we show a fatigue damage map of the stress hot spot for one of the hydrofoils of the rotor. We then explore the accuracy of the probabilistic method for a wider range of sea states. The sea states are simulated through JONSWAP wave energy spectra, which are simulated containing 80 discrete waves each with different phases. Therefore, we explore the limits of the probabilistic fatigue method for a wider range of sea state conditions.

C. Fatigue damage map

In this Section, we show the damage map for the hydrofoil stress hot spot in Figure 11. Damage values are computed through a deterministic approach and with the foil operating at optimal constant speed [10]. It can be seen, in Figure 11, that two damage peaks are identified, one at low rotational periods and intermediate wave heights (peak 1), and a second peak at high wave heights and intermediate rotational periods (peak 2).

The shape of Figure 11 is strongly determined by the probability distribution of the sea states. The first D peak is due to a combination of high probability of occurrence of sea states and high number of rotation cycles of the rotor due to low T_p. The second peak is due to higher wave heights in combination with the probability of occurrence. We note that the shape of Figure 11 changes for different installation sites and due to the distribution of the probability of occurrence. Hence, in the next Section, for the comparison analysis between deterministic and probabilistic fatigue methods, we consider the case where all sea states are granted equal probability of occurrence, and we assume that the rotor operates at constant rotational

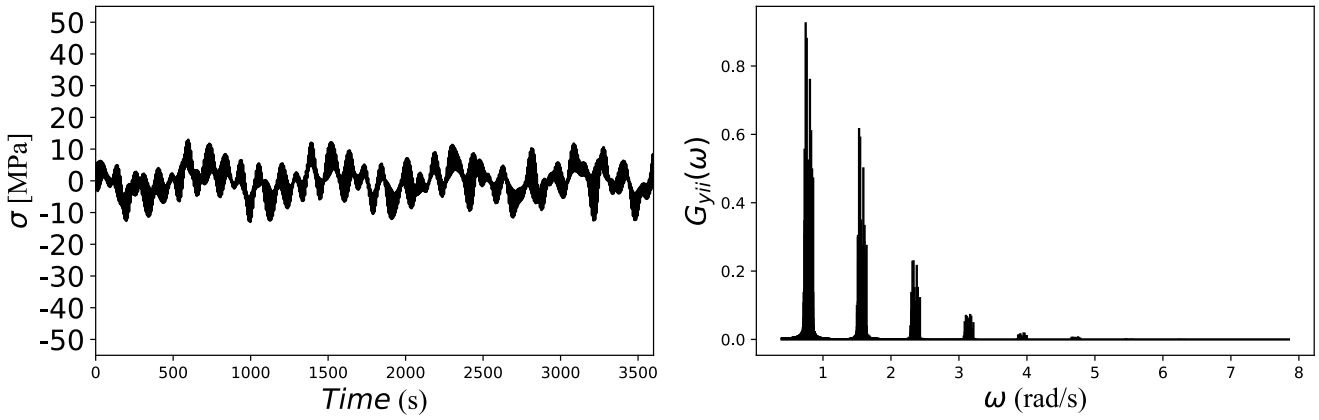

Fig. 7. a) σ time series in hydrofoil hot spot due to irregular sea state generated with a narrow band width of $0.9 \leq \omega \leq 1.1$ with 10 discrete waves and b) stress spectrum $G_{yyi}(\omega)$, where the first peak is $\omega_p = 0.78$ rad/s and the subsequent peaks are harmonics of the stress signal.

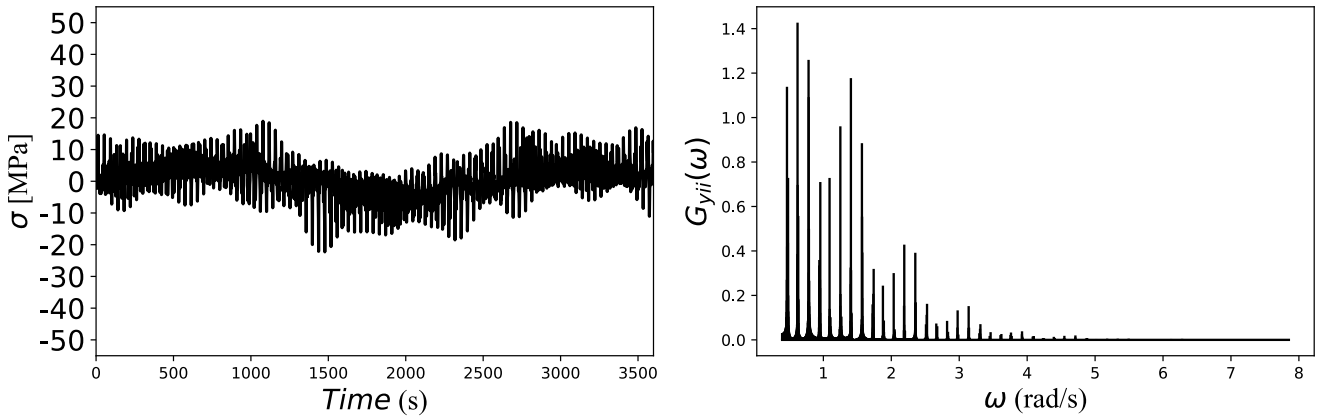

Fig. 8. a) σ time series in hydrofoil hot spot due to irregular sea state generated with a broad band width of $0.5 \leq \omega \leq 2.5$ with 10 discrete waves and b) stress spectrum $G_{yyi}(\omega)$, where the dominant peak is $\omega_p = 0.78$ rad/s and the shape of the spectrum is approximated with a Gaussian distribution.

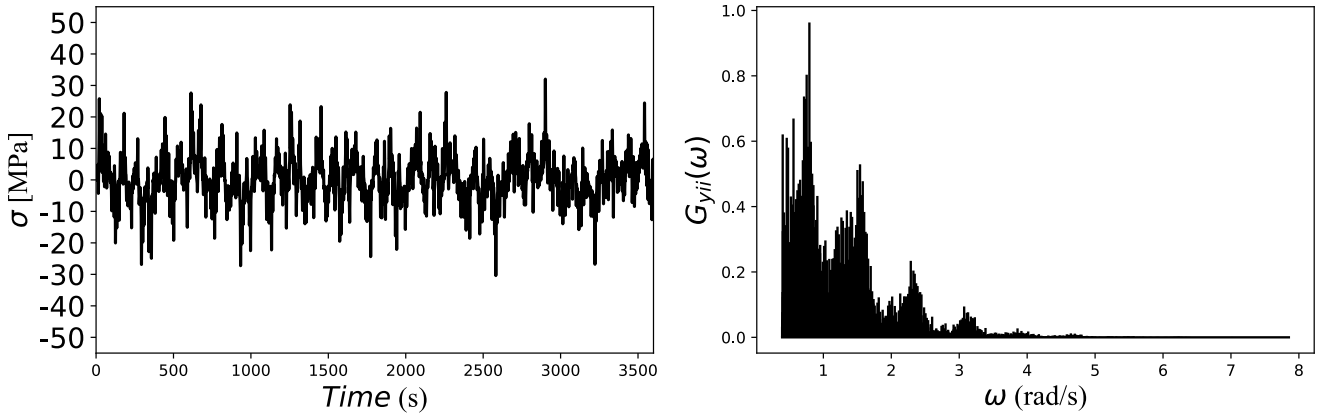

Fig. 9. a) σ time series in hydrofoil hot spot due to irregular sea state generated with a broad band width of $0.5 \leq \omega \leq 2.5$ with 80 discrete waves and b) stress spectrum $G_{yyi}(\omega)$, where the dominant peak is $\omega_p = 0.78$ rad/s and the shape of the spectrum is approximated with a Gaussian distribution.

velocity and equal to the peak frequency (ω_p) of the JONSWAP spectrum. The damage with probabilistic and deterministic methods is computed during 1 hour of simulations averaged over 20 trials.

D. Assessment of probabilistic fatigue method in different sea states

In this Section we compare the prediction capabilities of the probabilistic method to compute D at the hydrofoil stress hot spot for a different range of

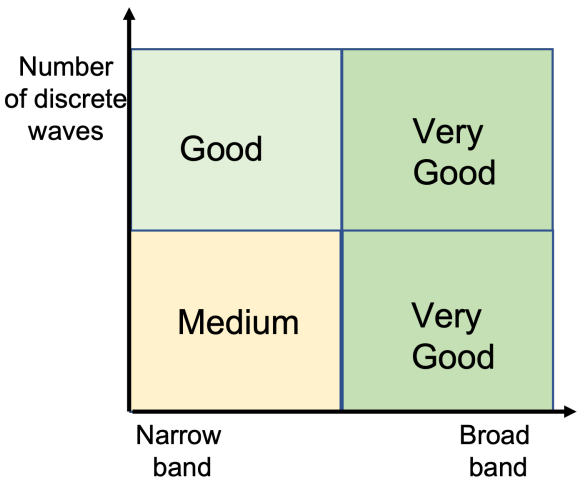

Fig. 10. Fuzzy chart showing level of agreement between probabilistic method and deterministic approaches to determine D in the foil hot spot. The horizontal axis shows the type of spectrum from narrow to broad band. The vertical axis shows the number of discrete waves used to produce the spectrum.

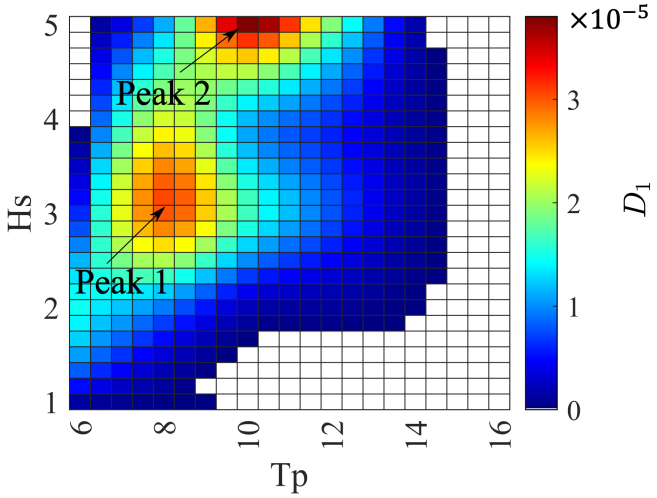

Fig. 11. Fatigue damage plot computed with the rotor operating at optimal rotational velocity, as computed in Arredondo-Galeana et al. [10].

sea states. We consider a JONWSWAP broad band spectrum composed of 80 discrete waves for each of the tested sea states. It is expected that for high probability sea states, i.e. $H_s \leq 3$ m and $T_p \leq 12$ s, the probabilistic method works satisfactorily. In contrast, for lower probability states, where the stress range might exceed the inflection point of the double slope SN-curve, the probabilistic method is expected to lose some of its accuracy.

The agreement between the probabilistic and the deterministic methods is determined through a traffic light color code, where green, yellow and red correspond to good, medium and low agreement. We use the ratio D_{prob}/D_{det} to determine the degree of agreement, where D_{prob} is the damage computed through the probabilistic method and D_{det} is the damage computed through Miner's rule. Here, $D_{prob}/D_{det} = 1$ shows the highest agreement. Note that both deterministic methods, the equivalent stress and Miner's rule, yield the same D_{det}, provided an appropriate selection of γ_i in the equivalent stress method.

Results are shown in Figure 12. We observe that for low probability sea states ($H_s \leq 3$ m and $T_p \leq 12$ s), the agreement is satisfactory, i.e. $D_{prob}/D_{det} \approx 1$. As the probability of the sea states decreases, i.e. as both H_s and T_p increase, D_{prob}/D_{det} decreases and drops to $D_{prob}/D_{det} \leq 0.8$. It is hypothesised that the agreement loses accuracy due to two main reasons. The first reason is because as H_s grows, there are stresses that exceed the inflection curve of a two slope SN curve. Secondly, as T_p increases, the non linearity of the spectrum increases and the accuracy of the probabilistic method deteriorates. Although, the comparison assessment is not dependent on the shape of the damage plot shown in Figure 11, it shows that probabilistic fatigue methods are an effective tool to predict damage accurately in a wide range of sea state conditions where lift based WECS might operate at.

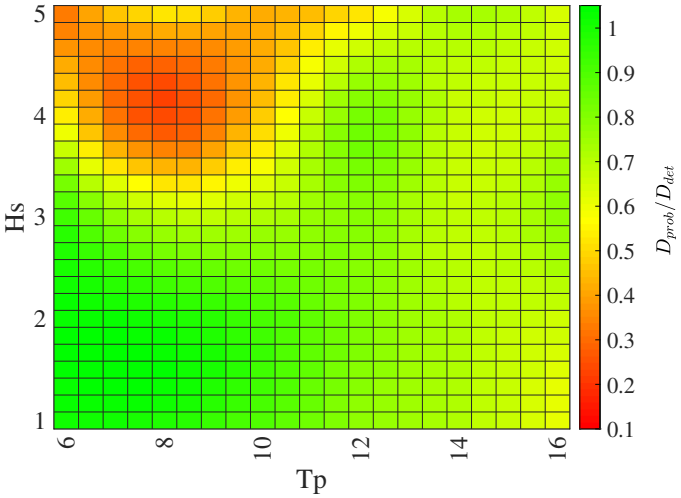

Fig. 12. Traffic light colour code plot showing agreement between probabilistic and deterministic methods through D_{prob}/D_{det} for a range of different sea state conditions.

VII. Conclusions

For high probability sea states, i.e. when the stress range is not likely to exceed the inflection point of a 2 slope SN curve, and when the rotor operates at at $T_p \leq 12$ s:

- The probabilistic method works well for a cyclorotor operating at constant rotational velocity in a broad band wave energy spectrum. Two broad band spectra are considered, one built with a reduced number of waves and one built with a large number of waves.
- The probabilistic method loses some accuracy, but still works reasonably well, for narrow band energy spectra that is built with a reduced number of waves.
- The method is less accurate for regular waves. The reason for this is still under investigation. One possible cause is that for regular sea states, the mean value of stresses in the foils is non

zero. However, the applicability of a probabilistic fatigue method to compute the damage due to a regular sea state is most likely of not practical use and therefore, not detrimental to the findings of this work.

Results shown in this paper highlight the feasibility of using probabilistic fatigue damage approaches in the study of damage of lift based WECs. This is a novel finding and opens a promising outlook towards the use of statistical analysis in the mechanical design and load analysis of such energy converters.

ACKNOWLEDGEMENT

The authors would like to thank all the members of the LiftWEC consortium for the fruitful discussion and input that has made this work possible. We would also like to thank the European Union's Horizon 2020 Research and Innovation Programme, which funded this project under Grant Agreement No 851885.

REFERENCES

[1] M. Jimenez-Martinez, "Fatigue of offshore structures: A review of statistical fatigue damage assessment for stochastic loadings," *International Journal of Fatigue*, vol. 132, p. 105327, 2020. [Online]. Available: https://www.sciencedirect.com/science/article/pii/S0142112319304311

[2] S. G. Siegel, "Numerical benchmarking study of a cycloidal wave energy converter," *Renewable Energy*, vol. 134, pp. 390 – 405, 2019.

[3] A. Ermakov and J. V. Ringwood, "A control-orientated analytical model for a cyclorotor wave energy device with n hydrofoils," *Journal of Ocean Engineering and Marine Energy*, vol. 7, no. 2, pp. 201–210, May 2021.

[4] A. Ermakov, F. Thiebaut, G. S. Payne, and J. V. Ringwood, "Validation of a control-oriented point vortex model for a cyclorotor-based wave energy device," *Journal of Fluids and Structures*, vol. 119, p. 103875, 2023. [Online]. Available: https://www.sciencedirect.com/science/article/pii/S0889974623000439

[5] A. Arredondo-Galeana, G. Olbert, W. Shi, and F. Brennan, "Near wake hydrodynamics and structural design of a single foil cycloidal rotor in regular waves," *Renewable Energy*, vol. 206, pp. 1020–1035, 2023.

[6] I. Rychlik and S. Gupta, "Rain-flow fatigue damage for transformed gaussian loads," *International Journal of Fatigue*, vol. 29, no. 3, pp. 406–420, 2007. [Online]. Available: https://www.sciencedirect.com/science/article/pii/S0142112306001769

[7] S. Siegel, "Wave climate scatter performance of a cycloidal wave energy converter," *Applied Ocean Research*, vol. 48, pp. 331–343, 2014. [Online]. Available: https://www.sciencedirect.com/science/article/pii/S0141118714001023

[8] J. Fernández-Chozas, A. Tetu, and A. Arredondo-Galeana, "Parametric cost model for the initial techno-economic assessment of lift-force based wave energy converters," in *Proceedings of the 14th European Wave and Tidal Energy Conference*, 2021.

[9] A. Arredondo-Galeana, W. Shi, G. Olbert, M. Scharf, A. Ermakov, J. Ringwood, and F. Brennan, "A methodology for the structural design of LiftWEC: A wave-bladed cyclorotor," in *Proceedings of the 14th European Wave and Tidal Energy Conference*, 2021.

[10] A. Arredondo-Galeana, A. Ermakov, W. Shi, J. V. Ringwood, and F. Brennan, "Control strategies for power enhancement and fatigue damage mitigation of wave cycloidal rotors."

[11] A. Ermakov, A. Marie, and J. V. Ringwood, "Optimal control of pitch and rotational velocity for a cyclorotor wave energy device," *IEEE Transactions on Sustainable Energy*, vol. 13, no. 3, pp. 1631–1640, 2022.

[12] S. Siegel, T. Jeans, and T. McLaughlin, "Deep ocean wave energy conversion using a cycloidal turbine," *Applied Ocean Research*, vol. 33, no. 2, pp. 110 – 119, 2011.

[13] A. Arredondo-Galeana and F. Brennan, "Floating offshore vertical axis wind turbines: Opportunities, challenges and way forward," *Energies*, vol. 14, no. 23, 2021. [Online]. Available: https://www.mdpi.com/1996-1073/14/23/8000

[14] R. E. Sheldahl and P. C. Klimas, "Aerodynamic characteristics of seven symmetrical airfoil sections through 180-degree angle of attack for use in aerodynamic analysis of vertical axis wind turbines," *Sandia National Laboratories.*, 3 1981.

[15] T. Jeans, C. Fagley, S. Siegel, and J. Seidel, "Irregular deep ocean wave energy attenuation using a cycloidal wave energy converter," *International Journal of Marine Energy*, vol. 1, pp. 16 – 32, 2013.

[16] M. L. Jalón and F. Brennan, "Hydrodynamic efficiency versus structural longevity of a fixed owc wave energy converter," *Ocean Engineering*, vol. 206, p. 107260, 2020.

[17] G. B. Airy, *Tides and waves*. Encyc. Metro., 1985, no. 192.

[18] M. McCormick, *Ocean wave energy conversion*, dover edition ed. Dover Publications Inc, 2013.

[19] J. V. Wehausen and E. V. Laitone, *Surface Waves*. Berlin, Heidelberg: Springer Berlin Heidelberg, 1960, pp. 446–778.

[20] J. Karlsson, K. Podgórski, and I. Rychlik, "The laplace multiaxial response model for fatigue analysis," *International Journal of Fatigue*, vol. 85, pp. 11–17, 2016. [Online]. Available: https://www.sciencedirect.com/science/article/pii/S0142112315004235

[21] M. Accensi and C. Maisondieu, "Homere. ifremer - laboratoire comportement des structures en mer." 2015.

[22] A. M. Cornett, "A Global Wave Energy Resource Assessment," ser. Proceedings of the Eighteenth International Offshore and Polar Engineering Conference, 08 2008.

[23] F. Ramos, S. López, E. Espinosa, J. Rebón, A. Hernández, and A. Arredondo, "Simulator for learning symbolically about the behavior of motion in bipedal robots," *International Journal of Engineering Education*, vol. 25, no. 2, pp. 250–260, Jun. 2009.